IJNAOE
©SNAK, 2015

Int. J. Nav. Archit. Ocean Eng. (2015) 7:833~847
http://dx.doi.org/10.1515/ijnaoe-2015-0059
pISSN: 2092-6782, eISSN: 2092-6790

Study on fatigue experiment for transverse butt welds under 2G and 3G weld positions

Sung-Wook Kang[1], Yong-Man Park[2], Beom-Seon Jang[1], Yu-Chul Jeon[3] and Seong-Min Kim[3]

[1]*RIMSE, Dept. of Naval Architecture and Ocean Engineering, Seoul National University, Seoul, Korea*
[2]*Dept. of Naval Architecture and Ocean Engineering, Seoul National University, Seoul, Korea*
[3]*Daewoo Shipbuilding & Marine Engineering Co., Ltd, Gyeongsangnam-do, Geoje, Korea*

Received 4 November 2014; Revised 22 April 2015; Accepted 24 June 2015

ABSTRACT: *Although the transverse butt weld method with ceramic backing strip has been widely used in various industrial fields for its fabricational convenience, it is rarely used in offshore industries since the fatigue strength of the weld joint has not been proved sufficiently. This study conducted fatigue tests for series of butt weld specimens with horizontal (2G) and vertical (3G) welding positions in order to verify the fatigue strength compared to S-N curve by DNV (Det Norske Veritas), IIW (International Institute of Welding) and Eurocode 3. The difference of the 2G specimens and the 3G specimens are investigated in terms of angular distortion and the effect on the fatigue strength are analyzed.*

KEY WORDS: Fatigue life; Weld position; Transverse butt weld; Ceramic backing strip; *Angular distortion.*

INTRODUCTION

A transverse welding method with a backing strip for the butt weld has been widely used in the construction of merchant ship due to its fabrication convenience as an alternative to a double-sided welding method. When the welding method is applied to thick plates requiring multi-pass welding and the backing material should be carefully chosen due to potential weld defects caused by burn-though, lack of fusion and incomplete penetration during the first pass. Therefore, it has been known for fatigue crack to occur in the vicinity of weld root due to the potential weld defects as shown in Fig. 1 (Maddox, 1991). For this reason, weld backing methods has been generally used to improve the welding quality on the weld roots. Kim investigated a few backing methods such as ceramic backing, water-cooled copper backing and no-backing method (Kim, 2010). Among the weld backing methods, the ceramic backing strip is known to be an efficient way with relatively low production cost where permanent backing strip is not admissible because of fatigue or corrosion. Kim et al. (2011) investigated the effect of various backing materials for butt weld joints in terms of fatigue strength. Four different cases of backing scenarios for butt-welded specimens such as steel backing, ceramic backing, no backing by cold metal transfer and under-matched welded specimen were investigated. No significant decrease in fatigue strength was observed when backing plates were steel backing and ceramic backing types. Kang et al. (2015) proposed a new method to remove weld scallops using an elongation of the v groove of the web plate to the face plate. In order to remove the weld scallop, a new wedge type ceramic backing method was developed.

Corresponding author: *Beom-Seon Jang*, e-mail: *seanjang@snu.ac.kr*

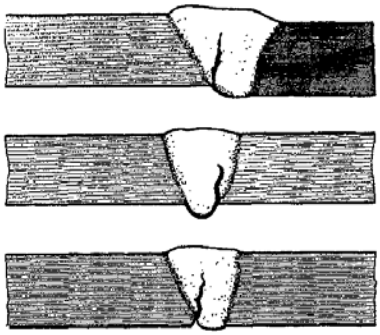

Fig. 1 General location of crack initiation on 1G specimen (Maddox, 1991).

In offshore structure, the use of transverse welding with the ceramic backing strip for thick plate has been started from the 1G flat position (see Fig. 2). Han et al. (2009) and Do et al. (2009) carried out fatigue experiments for a comparison of ceramic backing strip and steel backing plate in butt joints welded with 1G flat position. The results showed that sufficient fatigue lives could be achieved when using ceramic backing plate. In order for the welding method to be accepted for other welding positions such as 2G horizontal and 3G vertical positions in the conservative offshore field, exhaustive experimental studies need to be made further.

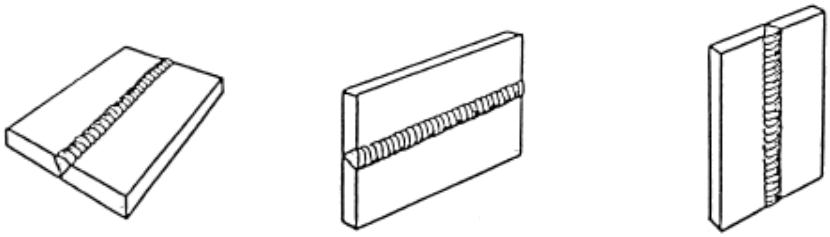

(a) 1G – Flat position. (b) 2G – Horizontal position. (c) 3G – Vertical position.

Fig. 2 Welding positions.

In this research, a fatigue experiment is performed to investigate the fatigue strength of transverse butt weld joints with temporary ceramic backing strip under 2G and 3G positions. The difference between 2G and 3G specimens are investigated in terms of angular distortion and the effect of the angular distortion on stress concentration and fatigue life are studied statistically.

EXPERIMENTS

Specifications of test specimens for fatigue test

In the present study, fatigue experiments are carried out on a total 40 transverse weld specimens. 20 specimens are welded under the 2G position, and the others under the 3G position, all with the ceramic backing strips. Here, flux-cored arc welding method is used. The material of the specimens is EH36 steel and thickness is 25 *mm*. The weld details for transverse butt joints have a groove angle and root gap of 40° and 6 *mm*, respectively. Table 1 provides the mechanical properties of base material (EH36) from mill test certificates and filler metal (E81T1-K2C). The shape and dimensions of the specimen is depicted in Fig. 3 and it is designed to satisfy the American Society for Testing and Materials standard (ASTM E466-96) represented in Fig. 4 (ASTM, 2002).

Table 1 Mechanical properties for base material and filler metal.

	Yield stress (*MPa*)	Tensile stress (*MPa*)	Elongation (%)
EH36	478	542	27
E81T1-K2C	470	550 - 690	19

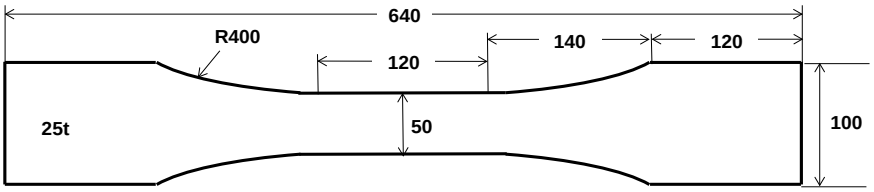

Fig. 3 Dimensions of specimen (EH36), thickness = 25 *mm.*

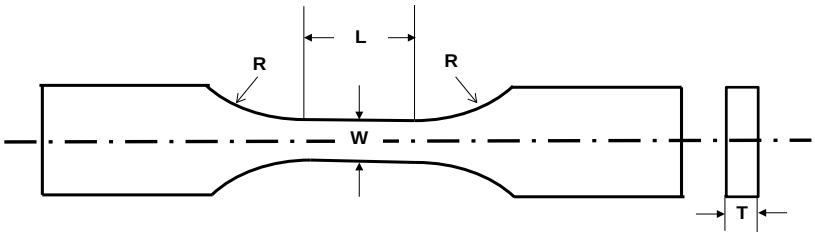

8W ≤ R, 2T ≤ W ≤ 6T, 2W ≤ L ≤ 3W
19.4mm² ≤ Reduced Area ≤ 645mm²

Fig. 4 ASTM standard for fatigue specimens.

Fig. 5 shows the shape of the bead and the welding path for 2G and 3G specimens. In both specimens, it is apparent that the bead on the ceramic backing plate side, weld root side, is smaller than that on the opposite side. For an experimental and analytical convenience, four locations are defined according to the bead size and weld path, as depicted in Fig. 6. Fig. 6 also shows the sequence of welding pass in accordance with the Welding Procedure Specification (WPS) of Daewoo Shipbuilding & Marine Engineering (DSME). The distinction between front and back sides is made according to the relative size of the bead, the larger bead side defined as the front side (F) and the smaller as the back side (B). The upper side (U) and lower side (L) are classified depending on the direction of the weld path.

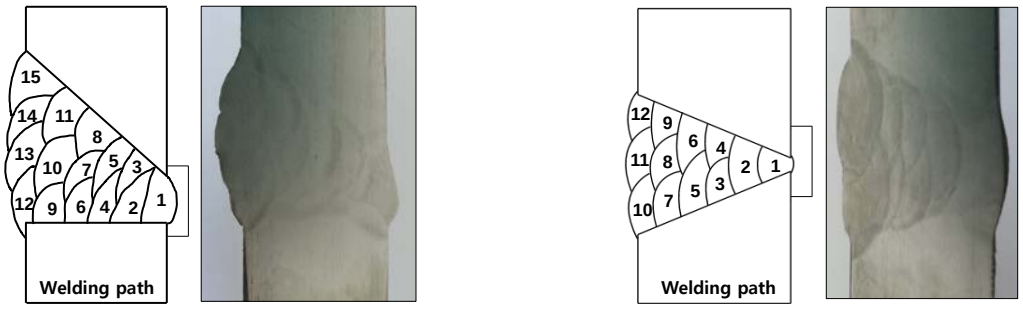

(a) 2G specimen. (b) 3G specimen.

Fig. 5 Welding paths and bead profiles of specimens.

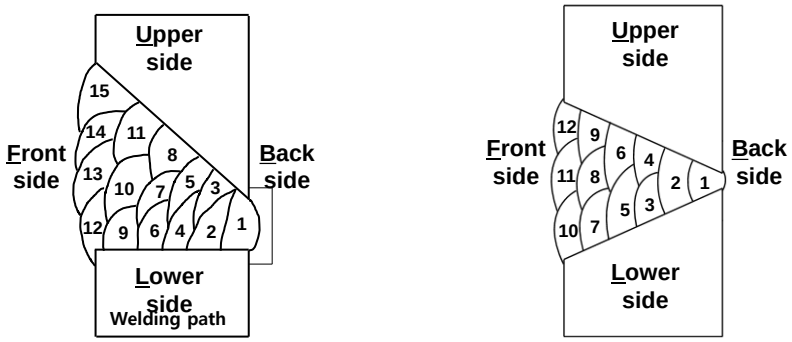

Fig. 6 Four directions of specimens.

Hot spots are defined at four ends of weld bead (FL, FU, BL and BU) as shown in Figs. 7 and 8. In order to calculate of hot spot stress in the specimen, the first and second gauges are affixed to each specimen at a distance of 0.5 *t* (12.5 *mm*) and 1.5 *t* (37.5 *mm*) from the weld bead (Hobbacher, 2008; Det Norske Veritas, 2010). Also, the gauge length in the experiment is used as 5 *mm* and it satisfies the IIW (International Institute of Welding) recommendation. Fig. 7 and Fig. 8 show the positions of the eight strain gauges attached to the 2G and 3G specimens, respectively.

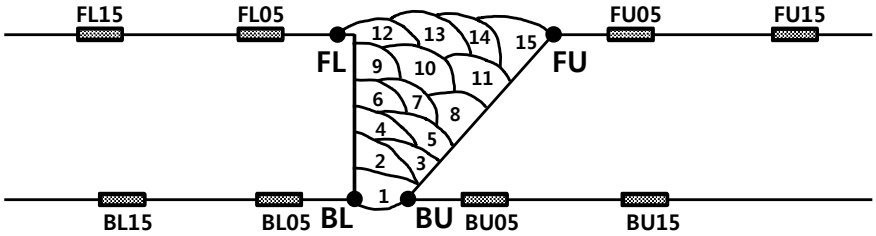

Fig. 7 Strain gauges attached to 2G specimen.

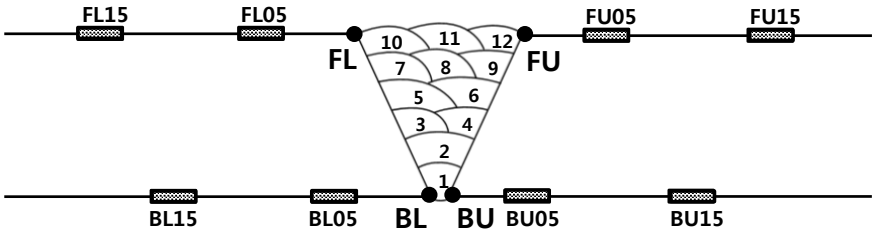

Fig. 8 Strain gauges attached to 3G specimen.

Specifications of experimental equipment for fatigue test

Fig. 9 shows equipment for fatigue experiment. The specifications of the test machine are summarized in Table 2.

Table 2 Specifications of the test machine.

Load (*kN*)	-500 ~ 500
Displacement (*mm*)	-125 ~ 125
Frequency (*Hz*)	Depend on load range
Control mode	load, displacement, elongation

Fig. 9 Fatigue experiment equipment.

3D Finite element analysis

In order to investigate the effect of weld beads on the stress concentration at the hotspots in advance, a finite element analysis is carried out. The zone in the vicinity of weld bead is scanned using a 3D scanner and modeled with sufficiently fine mesh using a commercial software HyperMesh (Altair Engineering, Inc, 2001) as depicted in Fig. 10. Three dimensional 4-node Tet4 elements were used for the part in the vicinity of weld bead and 8-node Hex8 elements for the other parts. The number of elements are 167,229. The other parts outside the weld bead are modeled as the drawing and the angular distortion is not reflected in the model.

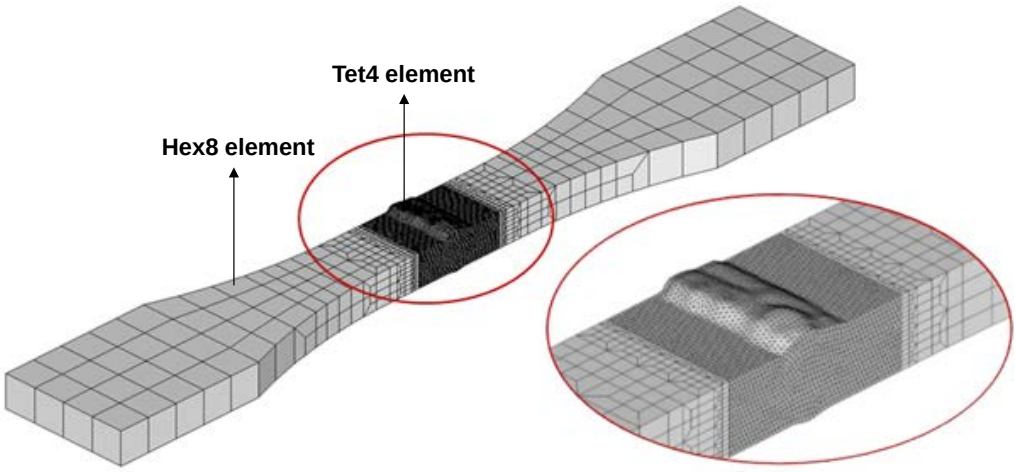

Fig. 10 Model of the 3G specimen for 3D FE analysis.

As shown in Fig. 11, a load of 31.6 *kN* is applied to each of 10 nodes (total 316 *kN*) which are located at the end of the specimen and the opposite nodes are fixed for all degrees of freedom. This load corresponds to a nominal stress of about 253 *MPa* and it is one of nominal stresses planned in the fatigue experiment. The finite element analysis is carried out using MSC.Nastran and the elastic modulus of the test specimens is assumed 210 *GPa*.

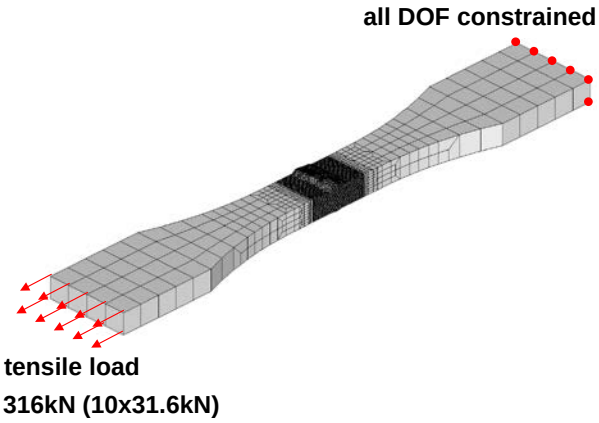

Fig. 11 Loading condition and boundary condition for 3D FE analysis.

Fig. 12 shows the results of finite element analysis. The calculated stresses are displayed at the locations of 0.5 *t* and 1.5 *t* and the hotspot stresses are calculated by linearly extrapolating those stresses. The calculated hotspot stresses are 255.2 *MPa* in FL and 254.18 *MPa* in FU, respectively. The corresponding Stress Concentration Factors (SCF) to be calculated by dividing the hotspot stresses by the nominal stress are 1.01 and 1.00, respectively. The stress concentration caused by the existence of the weld bead is quite small and negligible.

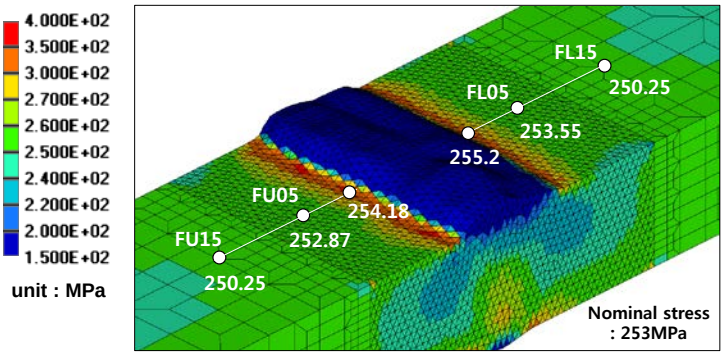

Fig. 12 Stress contour from the result of 3D FE analysis.

Angular Distortion measurement of specimen

The specimens were initially deflected slightly due to the heat imposed during the welding process and it can affect the hotspot stress and fatigue life. Thus, it needs to be carefully measured and the effect on the fatigue life to be examined carefully. All specimens have convex back side and concave front side. As shown in Fig. 13, when a specimen is mounted and seized by the grip, the angular distortion is straightened to a degree. Consequently, tensile stress and compression stress of about 200 *MPa* occur in the front side and the back side, respectively. This value corresponds to about 40% of the yield stress of EH36 steel. To analyze the effects of the angular distortion stress on fatigue life, the angular distortions are measured as shown in Fig. 14.

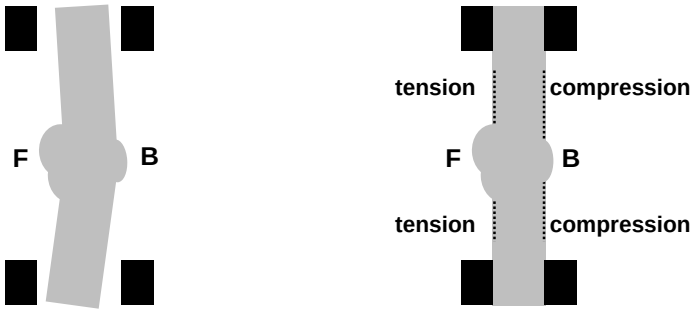

(a) Grip open. (b) Grip closed.

Fig. 13 Grip-induced tension and compression on specimen.

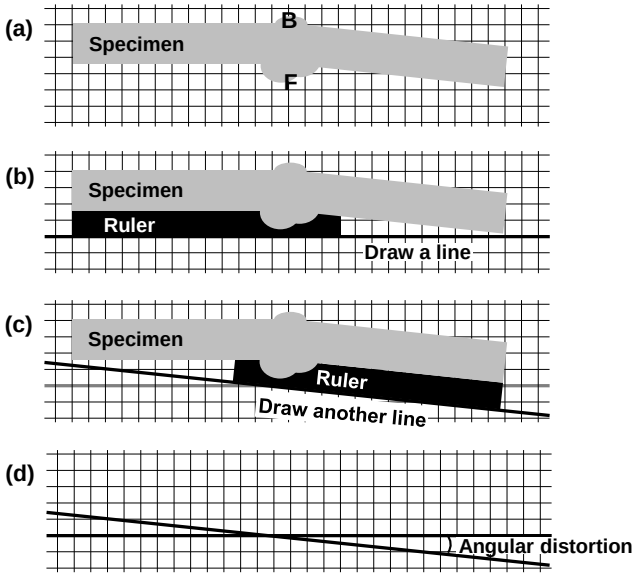

Fig. 14 Measurement of angular distortion of specimen.

The measurement procedure is explained in Fig. 14. This method is not a high-precision method obviously. The accuracy of the above method, therefore, is verified through an investigation of a correlation between the bending angle and the bending stress occurring when the specimen is seized by the grip. As shown in Fig. 15, the strain caused by the grip becomes larger as the angular distortion increases. Therefore, the use of the proposed method is deemed to be useful. For ten 2G specimens and eleven 3G specimens, the angular distortion angles are measured using the proposed method. For the 2G specimens, the angular distortion ranges from about 0° to 0.82°, and the average is 0.33°, while the 3G specimens from 0.82° to 2.12° with the average of 1.58°. The 3G specimens have about five times larger angular distortion than the 2G specimens.

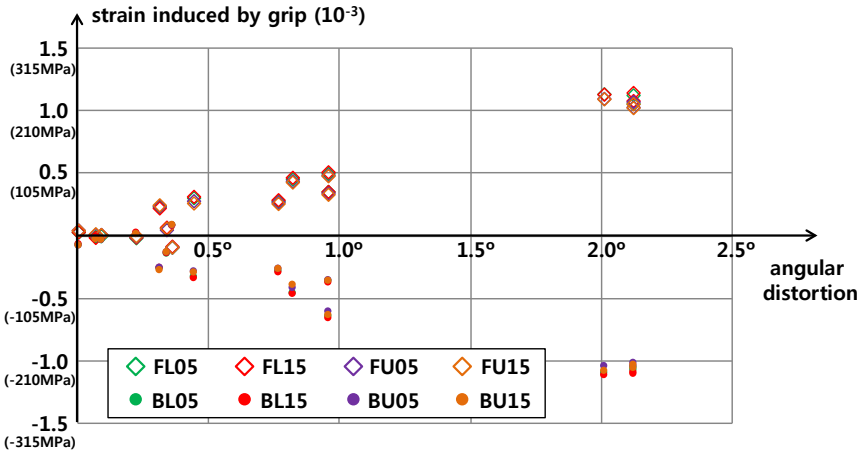

Fig. 15 Correspondence of strain induced by grip to angular distortion.

Fatigue test conditions

As shown in Table 1, the fatigue test is performed for nominal stress range of 120~330 *MPa*. These stress ranges (it is calculated by fatigue loading) are calculated based on the followings. According to the mill test certification of the test specimen, the yield stress is 478 *MPa*. Therefore, the maximum fatigue loading has to be less than 597.5 *kN* which leads to the yield stress. In addition, the maximum fatigue loading should be less than maximum loading capacity of equipment, 500 *kN*. Furthermore, for the safety reasons, the maximum fatigue loading value is determined as 434 *kN* and other fatigue loading cases are calculated as Table.1. The stress ratio is set 0.05 and the applied loads are calculated by multiplying the cross-sectional area (25 *mm* × 50 *mm*) of the specimen to the nominal stress. The experiments are conducted under load control. The applied load corresponds to 'load command' and the measured load to 'load feedback'. When the experiment is initiated, the controller starts to measure the maximum and minimum values of the load feedback for each cycle. The experiment is set to be terminated when the difference between the maximum or minimum values of the load feedback and the corresponding load command goes beyond 10% as illustrated in Fig. 16.

Table 1 Fatigue-test conditions.

Stress range [*MPa*]	Number of specimens	Stress [*MPa*]		Load [*kN*]		Frequency [*Hz*]
		Max	Min	Max	Min	
330	2	347	17	434	21	3
300	2	316	16	395	20	3
270	3	284	15	356	18	4
240	3	253	13	316	16	4
210	3	221	11	277	14	4 ~ 6
180	3	189	9	236	11	6 ~ 10
150	2	158	8	198	10	6 ~ 10
120	2	126	6	158	8	6 ~ 10

If specimen breakage occurs, the load feedback falls to zero, and the actuator is set to stop. Fig. 16 illustrates the termination of a test upon specimen breakage.

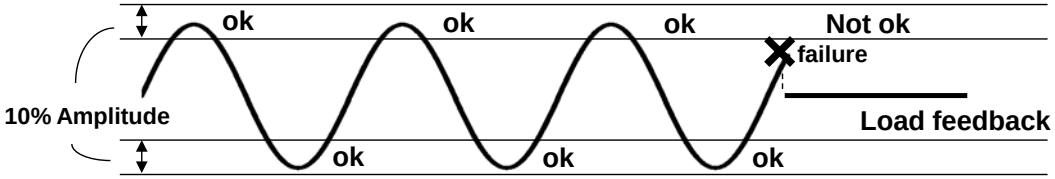

Fig. 16 Termination of test according to load feedback.

Fatigue test procedure

The overall experimental procedure is as follows.

1) The value of load cell is calibrated to zero using the offset of the self-weight of the upper grip.
2) The specimen is mounted on the grip.
3) After removing the load generated during the mounting process, and the strain gauge is calibrated to zero.
4) Depending on the stress range, the experimental frequency is set considering the capacity of actuator.
5) In order to make the load feedback coincide with the load command, tuning is performed.
6) The experiment is initiated.
7) If specimen reaches its failure, the experiment is automatically terminated.
8) If the number of load cycles goes beyond 5 million cycles, the experiment is stopped.

RESULTS AND DISCUSSION

Failure locations

The failure locations of the 2G and the 3G specimens are summarized in Table 2 and Fig. 17. In most specimens, the fatigue crack happens at the front side NOT at the backing plate side (weld root) differently from the reference (Maddox, 1991). The reason is due to the angular distortion. Tensional bending stress is added to the axial tension on the concave front side while compressive bending stress deducted on the convex back side. Even if the possibility of potential welding defects is higher at the weld root (the back side), the larger hot spot stress on the front side is more governing. This is to be investigated further in the following sections.

Among twenty 2G specimens, sixteen specimens failed at FL locations and two specimens at the middle of FU and FL locations ("FM"). The other one was terminated as the number of load cycles goes beyond 4.3 million. The front side cracks happened at the lower side (FL) not the upper side (FU). It is due to higher stress concentration factors of FL than FU and it can be explained by the asymmetric bead shape. It will be discussed again. One specimen having an opposite curvature (bent reversely) failed from the back side. In case of 3G specimen, due to the symmetric shape, the numbers of cracks from FL and FU are similar.

Table 2 Summary of fatigue failure locations for each specimen.

Failure location specimen	FU (Toe)	FL (Toe)	BL (Root)	BU (Root)	Remarks
2G Specimens	0	16	1	0	FM (Bead) : 2 Termination : 1
3G Specimens	11	7	0	0	Termination : 3

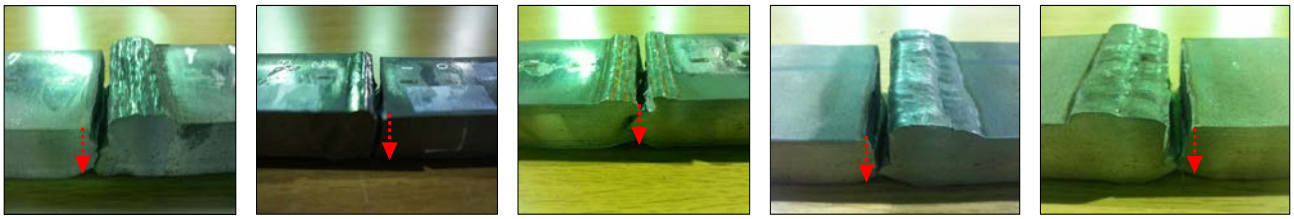

(a) 2G-FL: Toe crack. (b) 2G-BL: Root crack. (c) 2G-FM: Bead crack. (d) 3G-FU: Toe crack. (e) 3G-FL: Toe crack.

Fig. 17 Failure locations of test specimens.

Assessment of fatigue life (S-N curve)

The fatigue-experimental results are plotted on the logS – logN axis in Fig. 18. The linear regression lines are drawn using the least square method excluding the terminated specimens. The slope of the regression lines are set the same as that of DNV S-N curves. They are compared with DNV 'F' and 'W3' mean curves used for the single-sided transverse butt weld specimens among S-N curves of DNV-RP-C203 (Det Norske Veritas, 2010). DNV 'F' curve is used for a transverse butt weld on a temporary or a permanent backing strip without fillet welds and DNV 'W3' curve for a single-sided butt weld without backing strip. In addition, IIW 'FAT 80' and Eurocode 3 '71' curves are also compared. The 'FAT 80 class includes transverse butt weld, welded on non-fusible temporary backing and root crack (Hobbacher, 2008). Eurocode 3 '71' is for a transverse splice with backing strip (CEN, 2005). In Fig. 18, Eurocode 3 '71' curve and DNV 'F' curve are nearly the same.

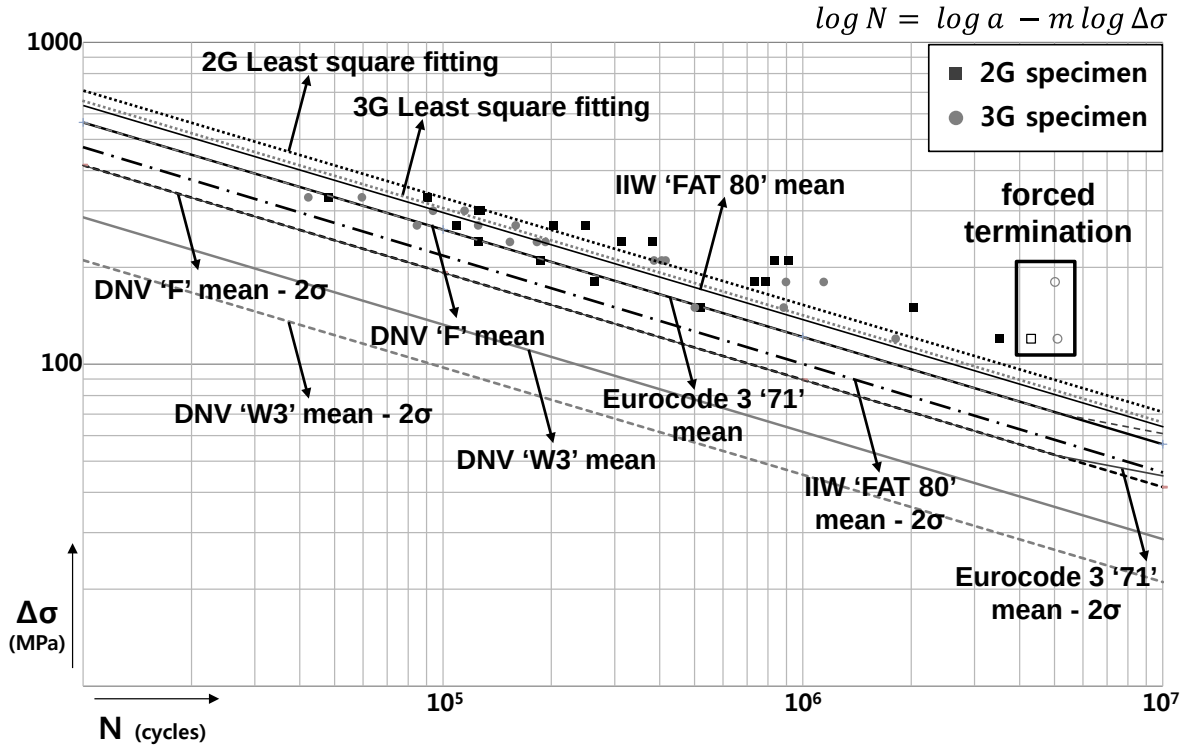

Fig. 18 Comparison of test results with the existing S-N curves.

As indicated in Table 3, the average fatigue life of the 2G specimens is longer than that of the 3G specimens. Also, both of the average fatigue lives of the 2G and 3G specimens are longer than DNV 'F', DNV 'W3', IIW 'FAT 80' and Eurocode 3 '71' mean curves.`

Table 3 Negative inverse slope and intercept of curves.

Types	Curves	*m*	*loga*
Mean curve	2G Least Square Fitting	3.0	12.548
	3G Least Square Fitting	3.0	12.451
	IIW 'FAT 80'	3.0	12.405
	DNV 'F'	3.0	12.255
	Eurocode 3 '71'	3.0	12.251
	DNV 'W3'	3.0	11.370
Mean -2σ on logN test data	IIW 'FAT 80'	3.0	12.005
	DNV 'F'	3.0	11.855
	Eurocode 3 '71'	3.0	11.851
	DNV 'W3'	3.0	10.970

Analysis of measured strain data

Four strain gauges located at the distance of 0.5 *t* and 1.5 *t* from a hotspot are compared in this section. The strains are the values when the load cycle reaches 10% of fatigue life. Figs. 19 and 20 plot the strain values from the strain gauges placed on the front side of the 2G and 3G specimens. It is identified that all of the strain values at 0.5 *t* position are larger than 1.5 *t*. After each specimen is grabbed by the grip, the strain gauges are calibrated to zero. Thus, the effect of angular distortion would disappear to a degree. However, the angular distortion is not completely eliminated and additional bending stress occurs when the tensional load is applied. Tensional bending stress occurs on the concave front side and compressive bending stress on the convex back side. The effect of angular distortion becomes larger as it approaches closer to the weld bead. The strain difference between at 0.5 *t* and 1.5 *t* of 3G specimens is larger than that of 2G specimens due to the larger the angular distortion.

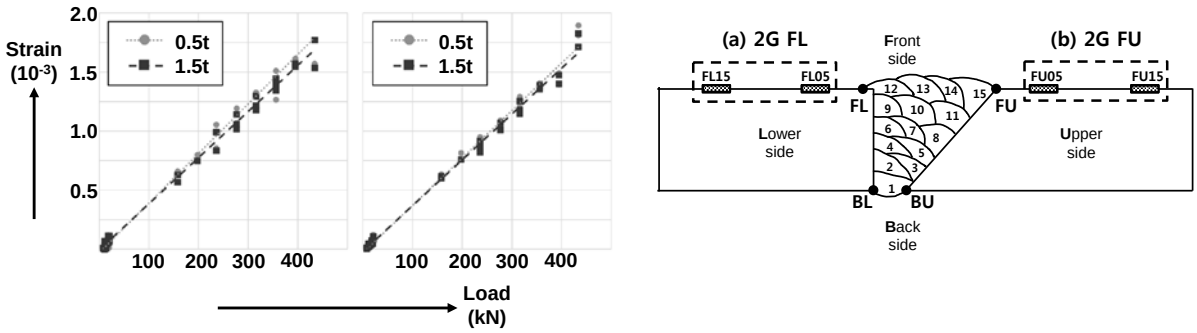

(a) 2G FL. (b) 2G FU. (c) 2G specimen.

Fig. 19 Strain data from front sides of 2G specimens.

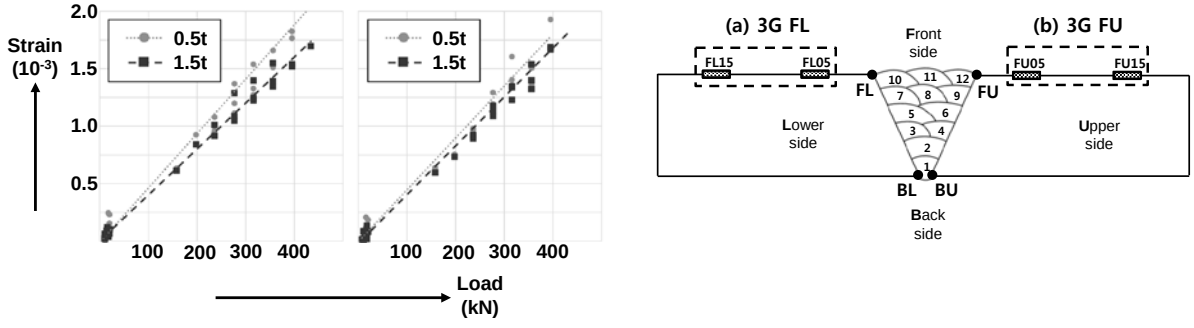

(a) 3G FL. (b) 3G FU. (c) 3G specimen.

Fig. 20 Strain data from front sides of 3G specimens.

For the back side, the strain values at 0.5 *t* are smaller than those at 1.5 *t* as depicted in Figs. 21 and 22. Larger compressive bending stress is deducted from the applied tensional load at 0.5 *t* than at 1.5 *t*. For the same reason, the difference between 1.5 *t* and 0.5 *t* is larger for the 3G specimens. However, the BU surface of 2G specimens is exceptional, that is, the strain at 0.5 *t* is slightly larger than 1.5 *t*. It can be explained by the asymmetric bead shape on the back side.

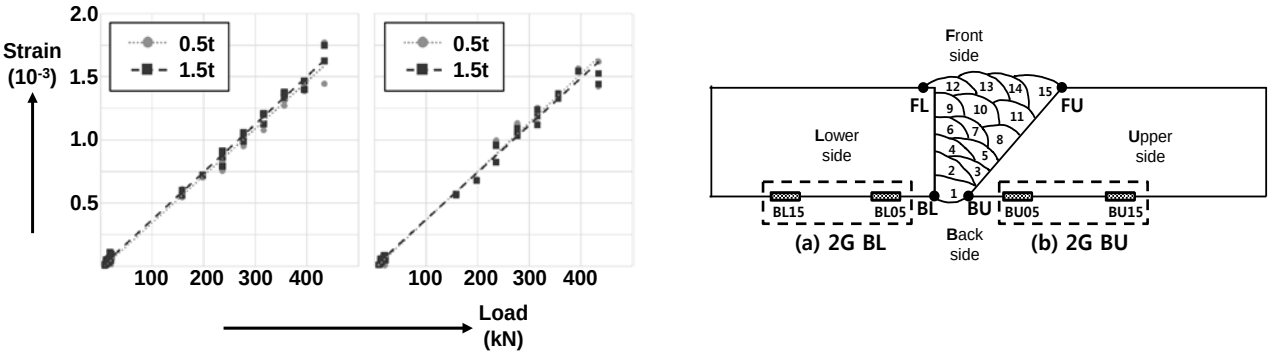

(a) 2G BL. (b) 2G BU. (c) 2G specimen.

Fig. 21 Strain data from back sides of 2G specimens.

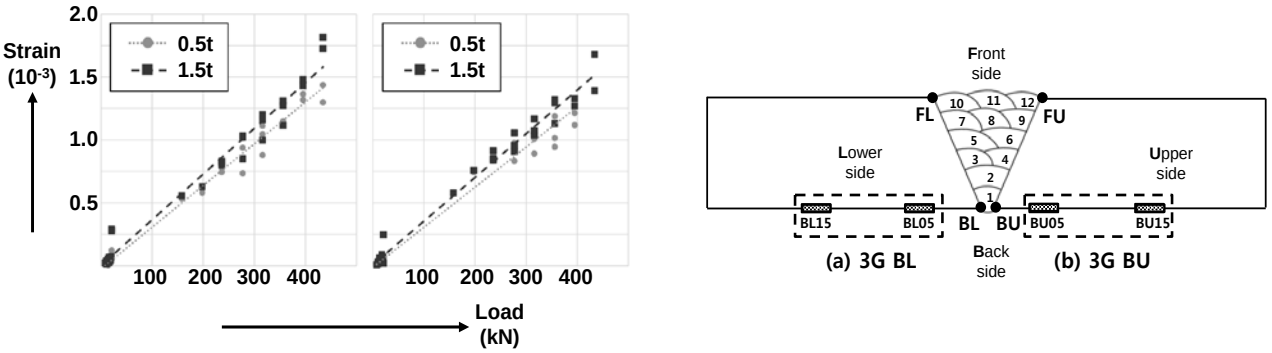

(a) 3G BL. (b) 3G BU. (c) 3G specimen.

Fig. 22 Strain data from back sides of 3G specimens.

The weld bead on the back side in the 2G specimens is asymmetric and biased to the lower side as shown in Fig. 23. When each specimen is unbent by the grip, the compressive bending stress at BU05 would be smaller than BL05 due to its larger section modulus. Thus, the resultant strain at BU05 is a little bit larger than BU15 differently from the BL side.

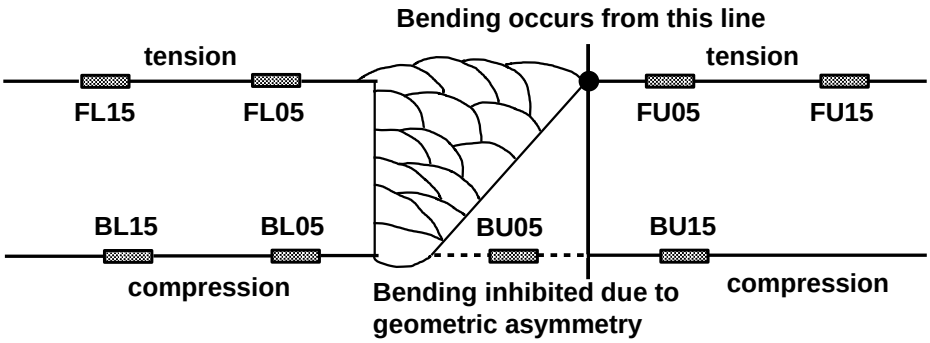

Fig. 23 Geometric asymmetry of 2G specimen's weld bead.

Calculation of stress concentration factor (SCF)

Fig. 24 shows SCF at hotspots for the 2G and 3G specimens. A hotspot stress is calculated by a linear extrapolation from stresses at 1.5 *t* to 0.5 *t*, and SCF at the hotspot is determined by dividing the hotspot stress by the nominal stress. The average SCF value is larger for the 3G specimens (1.24) than for the 2G specimens (1.09).

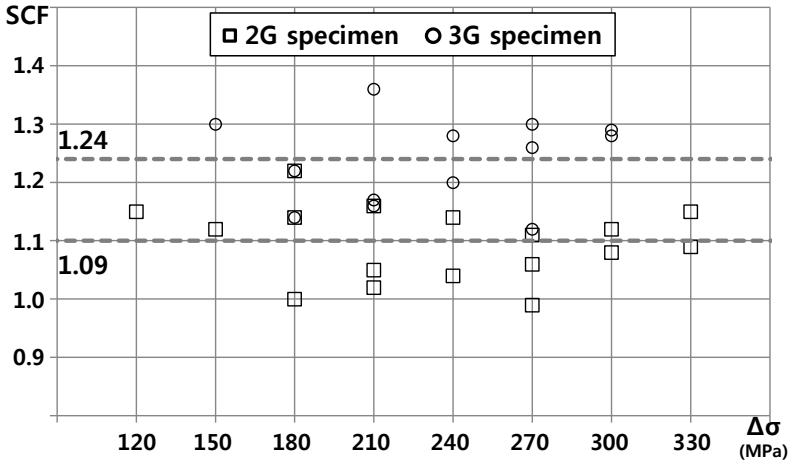

Fig. 24 SCF values for 2G and 3G specimens.

This result shows a big difference from the finite element analysis results in Fig. 12. The SCF calculated in the finite element analysis doesn't include the angular distortion effect. Only the effect of bead shape is reflected into the calculation and the resultant SCFs were found to be quite small. The differences between the nominal stress and the stresses at 1.5 *t* and 0.5 *t* are below 1% of nominal stress. Therefore, the angular distortion is the main contribution to the stress concentration rather than the bead shape.

Fig. 25 shows a strong correlation between the angular distortion and the SCF and it explains more clearly the angular distortion is the governing factor to stress concentration. It seems reasonable that the SCF values of 3G specimens with larger angular distortion are found to be larger than those of 2G specimens.

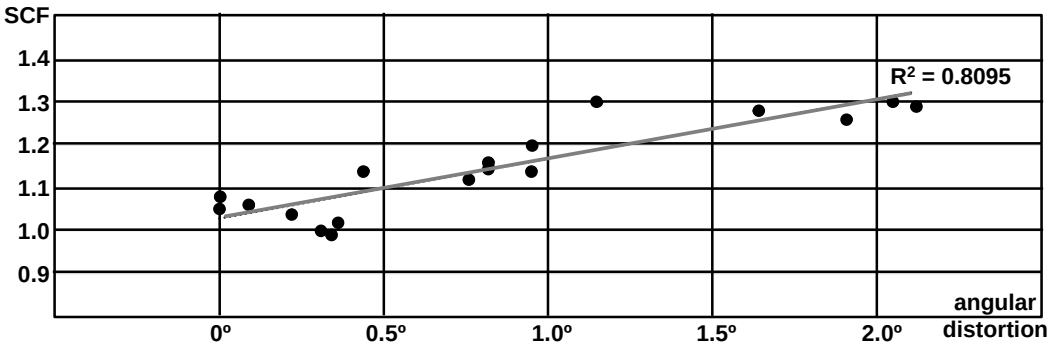

Fig. 25 Correlation between angular distortion and SCF.

Effect of angular distortion on fatigue life

The fatigue lives of the 2G specimens were assessed longer than those of the 3G specimens, which was caused by the larger angular distortion and SCF of the 3G specimens. In order to confirm the effect of angular distortion on the fatigue life, the S-N trend line is drawn for all of the specimens irrespective of the weld position (2G or 3G). The angular distortion angle of each specimen is marked in Fig. 26 and the level of angular distortion is distinguished by different symbols in Fig. 27.

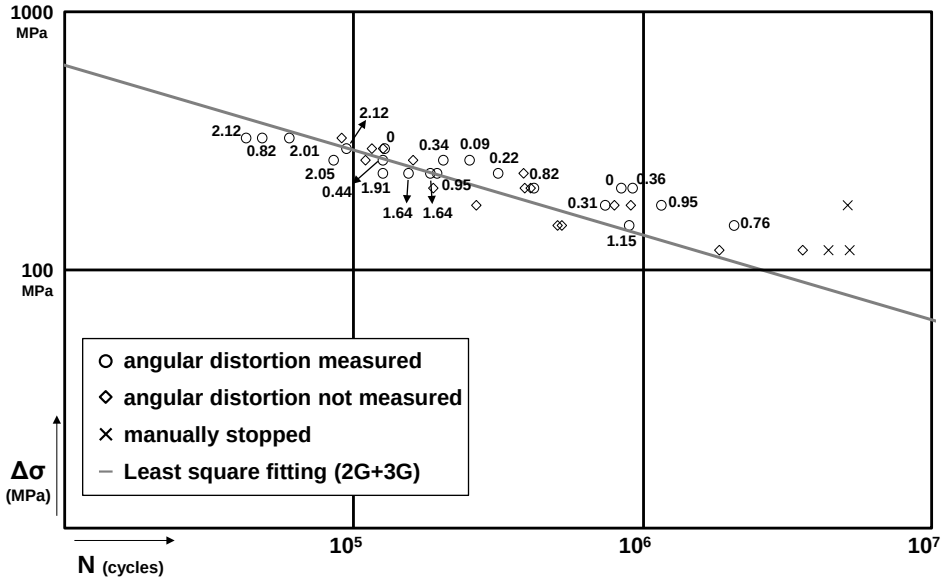

Fig. 26 Least square fitting and individual values of angular distortion of specimens.

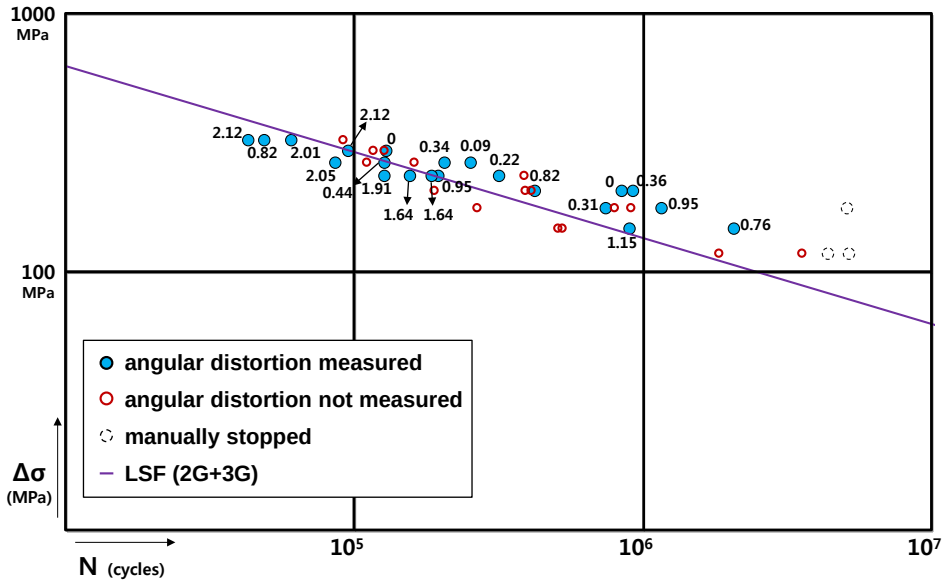

Fig. 27 Separate visualization of fatigue life classified by angular distortion.

With reference to the trend line, points with smaller angular distortion angle are positioned above the line and points with larger angle below the line. However, it is observed that the deviations decrease as the applied stress grows. It means that the effect of angular distortion on the fatigue life varies depending on the magnitude of applied load. This can be identified in the correlation between the deviation distance and the angular distortion or the nominal stress. The deviation distance is defined as the normal distance from a point to the regression line on the logS – logN scale. A point above the line has a positive deviation and a point below the line a negative deviation.

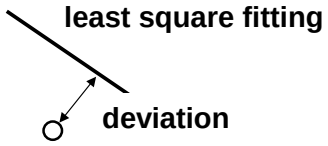

Fig. 28 Definition of deviation of fatigue life.

Fig. 29 shows the correlation between the deviation distance and the angular distortion, and Fig. 30 shows the correlation between the deviation distance and the SCF. The angular distortion and the deviation distance have a negative correlation. The SCF having a strong proportional relation with the angular distortion also has a negative correlation with the deviation distance. This means that larger SCF leads to higher hotspot stress and lower fatigue life.

Fig. 31 shows a negative correlation between the stress range and the deviation distance. It is because the ratio of bending stress to total stress becomes smaller as the nominal stress grows. It results in smaller stress concentration and less degradation of fatigue life.

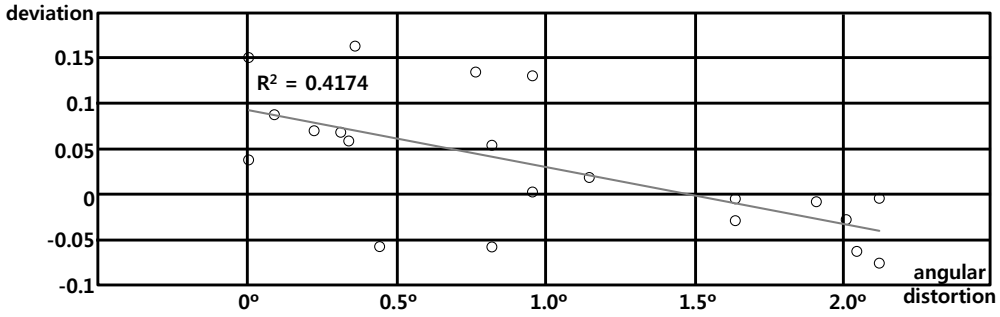

Fig. 29 Correlation between angular distortion and deviation.

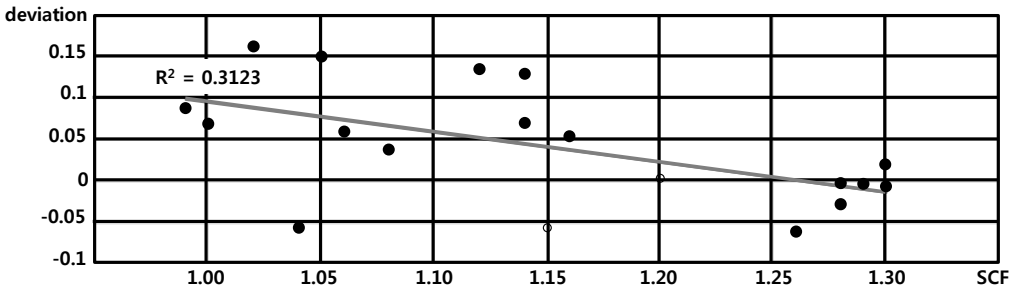

Fig. 30 Correlation between SCF and deviation.

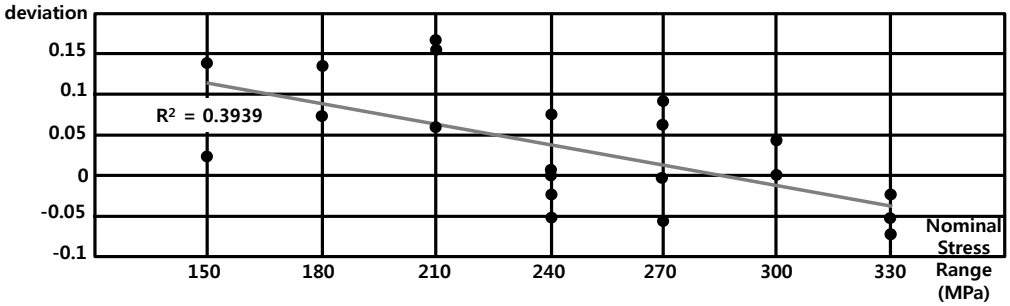

Fig. 31 Correlation between stress range and deviation.

The correlation of the angular distortion angle and the SCF or is considerably strong, as shown in Fig. 25. By contrast, the correlations among fatigue life, angular distortion, and stress range are relatively weak. Whereas the angular distortion and the strain values are directly related fatigue life is affected by various factors such as residual stress or welding defects as well as the angular distortion.

CONCLUSIONS

In the present study, fatigue experiments on twenty 2G and twenty 3G transverse butt weld specimens with ceramic backing plate are carried out. The findings are listed below.

- Prior to the fatigue experiment, finite element analysis was carried out for a 3G specimen. Since the actual angular distortion was not reflected in the finite element model, stress concentration caused by only the weld bead shape could be estimated. The effect of the weld bead on the stress concentration was found to be negligible.
- After the welding process, angular distortion occurs. The front side becomes convex and the back side concave since more heat is applied to the front side. The effect of the angular distortion was identified to be governing to the stress concentration at hot spots by investigating the relation between measured bending angles and SCFs.
- As the angular distortion of the specimen gets larger, the stress differences between the positions and the SCF become greater. Thus, fatigue life is shortened. It is found that the effect of the angular distortion on the reduction of fatigue life decreases as the stress range increases.
- In most specimens, fatigue crack occurred at the concave front side not at the back side. It is mainly due to its larger surface stress where the tensile bending stress induced by the angular distortion is added. However, this conclusion is valid to an individual specimen where the absence of external restraints by neighboring structure allows large angular distortion. When a butt-welded plate is connected to other structural member, its angular distortion can be suppressed to a degree. Further experiment and study is required for this case.
- The fatigue lives of the 2G specimens were measured to be longer than that of the 3G specimen, because the angular distortion of the 2G specimen is relatively smaller than the 3G specimen. However, both 2G and 3G specimens are found to have longer fatigue lives than that suggested by the DNV, IIW, Eurocode 3's criteria.

  Conclusively, the transverse welding with ceramic backing strip provides sufficient fatigue strength compared to the design curve (DNV, IIW, Eurocode 3's criteria).

ACKNOWLEDGEMENT

This research is supported by the New & Renewable Energy of the Korea Institute of Energy Technology Evaluation and Planning (KETEP) grant funded by the Korea government Ministry of Knowledge Economy (No. 20123010020090). In addition, this work was supported by Daewoo Shipbuilding & Marine Engineering Co., Ltd.

REFERENCES

Altair Engineering, Inc, 2011. *Altair hyermesh version 11.0 User Guide.* Michigan, USA: Altair Engineering, Inc.

ASTM, 2002. *Standard practice for conduction force controlled constant amplitude axial fatigue tests of metallic materials. E 466-96*. West Conshohocken, USA: ASTM.

CEN, 2005. *EN-1993-1-9: Eurocode 3: Design of steel structures, Part 1-9: Fatigue.* Brussels, Belgium : European Committee for Standardization.

Det Norske Veritas, 2010. Fatigue design of offshore steel structures. DNV-RP-C203. Høvik, Norway: Det Norske Veritas

Do, H.D., Kang, S.W., Han, J.H., Kim, S.M. and Kim, M.H., 2009. Fatigue assessment in accordance with back plate of butt welded specimens. *Journal of the Society of Naval Architects of Korea*, 46(1), pp.24-30.

Han, J.H., Kim, S.M., Lee, W.I., Kang, S.W. and Kim, M.H., 2009. Fatigue assessment of butt welded specimen according to the existence of the backplate. *Journal of Korean Welding and Joining Society*, 27(1), pp.90-94.

Hobbacher, A., 2008. *Recommendations for fatigue design of welded joints and components*. Paris, France: International Institute of Welding.

Kang, S.K., Yang , J.S., and Kim, H.K., 2015. Development of method to remove weld scallop and ceramic backing material of wedge type and its application. *International Journal of Naval Architecture and Ocean Engineering* , 7, pp. 315-323.

Kim, C.H., 2010. Back bead characteristics during butt welding of a thick plate for various backing conditions. *Materials Science Forum*, 654-656, pp.350-353.

Kim, M.H., Kim, H.J., Han, J.H., Lee, J.M., Kim, Y.D., Kang, N.H., Kang, M.J. and Kim, C.H., 2011. Influence of backing materials towards the fatigue strength of butt-welded joints. *Journal of Mechanical Engineering Science*, 225(8), pp. 1798-1807.

Maddox, S.J., 1991. *Fatigue strength of welded structures*. Cambridge: Abington Publishers.